

Journal of Biomedical Optics

SPIDigitalLibrary.org/jbo

New closed-form approximation for skin chromophore mapping

Petri Välisuo
Ilkka Kaartinen
Valery Tuchin
Jarmo Alander

New closed-form approximation for skin chromophore mapping

Petri Välisuo,^a Ilkka Kaartinen,^b Valery Tuchin,^c and Jarmo Alander^a

^aUniversity of Vaasa, Department of Electrical and Energy Engineering, Automation Technology, Wolffintie 34, Vaasa, 65101 Finland

^bTampere University Hospital, Department of Plastic Surgery, Tampere, Finland

^cSaratov State University, Institute of Precise Mechanics and Control of RAS, Saratov, Russia

Abstract. The concentrations of blood and melanin in skin can be estimated based on the reflectance of light. Many models for this estimation have been built, such as Monte Carlo simulation, diffusion models, and the differential modified Beer–Lambert law. The optimization-based methods are too slow for chromophore mapping of high-resolution spectral images, and the differential modified Beer–Lambert is not often accurate enough. Optimal coefficients for the differential Beer–Lambert model are calculated by differentiating the diffusion model, optimized to the normal skin spectrum. The derivatives are then used in predicting the difference in chromophore concentrations from the difference in absorption spectra. The accuracy of the method is tested both computationally and experimentally using a Monte Carlo multilayer simulation model, and the data are measured from the palm of a hand during an Allen's test, which modulates the blood content of skin. The correlations of the given and predicted blood, melanin, and oxygen saturation levels are correspondingly $r = 0.94$, $r = 0.99$, and $r = 0.73$. The prediction of the concentrations for all pixels in a 1-megapixel image would take ~ 20 min, which is orders of magnitude faster than the methods based on optimization during the prediction. © 2011 Society of Photo-Optical Instrumentation Engineers (SPIE). [DOI: 10.1117/1.3562976]

Keywords: diffusion theory; Monte Carlo methods; Beer–Lambert law; integrating sphere biomedical engineering; optics; photonics; biological tissues; multispectral imaging; medical imaging; dermal imaging.

Paper 10651R received Dec. 10, 2010; revised manuscript received Feb. 16, 2011; accepted for publication Feb. 17, 2011; published online Apr. 7, 2011.

1 Introduction

The reflectance spectra of human skin can be used to study its physical structure and chemical contents. The reflectance spectra measurement is a fast and convenient method for obtaining dermal information. The spectra can be measured using a spectrophotometer or with a multiband digital imaging device. In reflectance spectroscopy, the skin is illuminated with a light source and the spectra of the reflected light is measured. Often visible and near-infrared (NIR) light are used for measurements because they penetrate deeper into the skin than the longer or shorter wavelengths. The measured reflectance spectra can be used in estimation of the distributions of the skin chromophores, such as melanin and hemoglobin. These chromophore maps may help in diagnosing and following up on skin disorders. Therefore, chromophore mapping is a common topic in the skin-imaging literature.^{1–7} Several commercial technologies have been developed especially for measuring the skin chromophore concentrations, such as DermaSpectrometer[®], Mexameter[®], Chromameter[®],⁶ EMM-01,⁷ SIAScopy[®],⁸ and TIVI[®] imaging.⁹ Comparative measurements of erythema and melanin indexes using the EMM-01 and Mexameter MX-16 (Courage + Khazaka electronic GmbH, Cologne, Germany) devices as well as color measurements with the Minolta Chromameter CR-200b (Higashi-Ku, Japan) were performed in Ref. 7.

Because the light interaction in skin is complicated, there is no single method for chromophore concentration estimation that is the best for all purposes. Therefore, many different methods are frequently used in skin analysis. These methods are listed in recently published reviews.^{10,11} One of the most versatile methods for this purpose is Monte Carlo simulation, for example, the Monte Carlo multilayer (MCML) software.^{12–14} It is relatively easy to include the absorption of all important skin chromophores and scattering factors into the model. Notwithstanding the long simulation times, the model has been used for many purposes, such as in the development of the pulse oximeter,¹⁵ melanoma diagnostics,^{16–18} melanin- and blood-concentration measurements,^{19,20} skin-treatment planning,²¹ and determination of the information depth of the skin reflectance.²²

Another often-used method for modeling light transport in skin is the diffusion approximation of the light transport equation.^{23,24} Diffusion approximation is expressed as a mathematical formula that can be calculated much faster than the MCML model but it is less versatile. However, solving of inverse problems is required by means of an optimization algorithm, such as that of Levenberg–Marquardt (LMA).

Most solutions, aiming at even faster processing, are based on the Beer–Lambert law (BLL), which is the profound theory behind chemometry. The BLL states that the absorption A , of light transmitted through a substance, whose thickness is d is

Address all correspondence to: Petri Välisuo, University of Vaasa, Department of Electrical and Energy Engineering, Automation Technology, Wolffintie 34, Vaasa, Lnsi-Suomi 65101 Finland. Tel: 358445804320; Fax: 358-6-324 8677; E-mail: petri.valisuo@uwasa.fi.

directly proportional to the absorption coefficient, μ_a of the substance.

$$A = \mu_a d. \quad (1)$$

The absorption coefficient is the product of the molar extinction coefficient ε and the concentration c of the chromophore

$$\mu_a = c \varepsilon. \quad (2)$$

This law strictly holds only for light transmission when scattering is negligible. However, the scattering in skin is strong; thus, Beer–Lambert as such does not hold. On the other hand, the backscattering makes it possible to use the reflection-measurement setup instead of transmission, which is much more convenient for *in vivo* measurements. The goal for many researchers has been to modify either the BLL or the reflectance-measurement setup so that the BLL could be applied.

In scattering media, the photons do not follow direct path. Therefore, the thickness, d , must be replaced with a mean pathlength, p , of the photon, which is usually unknown, and depends on the absorption and scattering. Furthermore, photons are scattered in all directions, and only a small amount of them are captured by the detector, resulting in a scattering loss, which is often modeled as an additive term G . The modified Beer–Lambert law (MBLL), takes also into account these additional parameters,^{25,26}

$$A = \mu_a p + G. \quad (3)$$

Because of the constant, unknown term, G , the absolute absorption coefficient values cannot be solved from known absorptions. If it is assumed that the scattering loss is constant, then the term G disappears when examining the differences of absorptions. Therefore, the MBLL is often used in a differential form, known as differential modified Beer–Lambert law (dMBLL),

$$\frac{\partial}{\partial \mu_a} A = \frac{\partial}{\partial \mu_a} \mu_a p. \quad (4)$$

The dMBLL, shown in Eq. (4), is described in Ref. 27, as well as the error caused by assuming G as constant when it is not. If the pathlength, p , is not dependent on μ_a , then the derivative of absorption is just the pathlength and the dMBLL is linear. If either p or G is dependent on μ_a , both A and $\partial A / \partial \mu_a$ are nonlinear. In many papers, $\partial A / \partial \mu_a$ is assumed to be linear.^{3,27–29}

Mourant et al. found that in a special measurement setup, where light is illuminated from one optical fiber and collected from another so that the distance between the fibers is between 1.5 and 2.2 mm, the mean pathlength of the photons is only slightly dependent on the changes on the scattering coefficient.³⁰ In this case, the dMBLL holds well, provided that the $p(\mu_a)$ can be modeled. Mourant et al. used a model $p(\mu_a) = x_0 + x_1^{-x_2 \mu_a}$, where x_i are experimental coefficients.

Amelink and Sterenberg³¹ made a special measurement device where light is fed using one emitter fiber and detected by two fibers, simultaneously. The first detector fiber (d_e) is the emitter fiber itself, and the second (d) is a separate fiber located close to the emitter. The difference of the two detected signals is

said to mostly contain the effect of the single scattered photons. In this case, the average pathlength p is constant, the dMBLL is linear, and actually, the Beer–Lambert could be applied as such.³¹

Unfortunately, these special measurement setups cannot be used for chromophore mapping because they lack the spatial dimensions. A method that is fast and accurate enough for chromophore mapping of images with high spatial and modest spectral resolution is needed in a skin-imaging system, such as the Spectrocutometer.^{4,32} The new approach taken in this paper is to apply dMBLL to solve chromophore maps from digital images, linearizing the dMBLL model around an operating point deduced from the normal skin spectra of the individual. For the linearized model the partial derivatives of the absorption by the absorption coefficients of each chromophore are needed. These derivatives are obtained by constructing a two-layer skin model using the Beer–Lambert law and diffusion model and by differentiating the model analytically. The constructed model is first fitted to one selected absorption spectrum, using LMA optimization, to find the chromophore concentrations. The derivatives are then used to find the differences of the chromophore concentrations for the other spectra using dMBLL in closed form. The method is tested by comparing it to the MCML simulation model.

2 Materials and Methods

Melanin, oxyhemoglobin, and deoxyhemoglobin are the most important chromophores in skin. In healthy skin, melanin is deposited in epidermis, whereas hemoglobin is dissolved in blood, which is located deeper in the skin, in the dermis. The absorption of the epidermis is $\mu_{a,e} p_e$, where $\mu_{a,e} = c_m \varepsilon_m$ is the absorption coefficient of epidermis, which equals to the concentration of melanin, c_m , times the extinction coefficient of melanin, ε_m . The absorption coefficient of blood, μ_b , depends on the absorption coefficients of the chromophores in blood, oxygenated hemoglobin, μ_{a,HB_o} , and deoxygenated hemoglobin, μ_{a,HB_d} . The absorption of blood is therefore $\mu_{a,b} p_d = (\mu_{a,HB_o} + \mu_{a,HB_d}) p_d$ where p_d is the average pathlength of photons in dermis. Usually, the absorption coefficient of dermis itself, is modeled as skin baseline, $\mu_{a,d} p_d$. Therefore, the equation describing the attenuation of skin, can be written as follows:

$$A = \mu_{a,e} p_e + \mu_{a,b} p_d + \mu_{a,d} p_d + G. \quad (5)$$

The epidermis is weakly absorbing by itself, but the melanin deposited primarily in the bottom of the epidermis, in *stratum basale*, absorb light strongly. Because the epidermis is thin, $d_e \approx 100 \mu\text{m}$, and it is the topmost layer, the mean pathlength of a remitted photon in the epidermis is not affected much by the absorption of dermis or epidermis. Therefore, the derivative of Eq. (5) by the absorption in the epidermis, is approximately

$$\frac{\partial A}{\partial \mu_{a,e}} \approx p_e. \quad (6)$$

On the other hand, the mean pathlength in dermis, p_d , is dependent on the absorption coefficient in blood and in dermis. If $\mu_{a,b}$, is high, then only the photons remitted from the superficial layers in the dermis will survive back and the average pathlength in the dermis will be short. Therefore, the derivative of Eq. (5)

by the absorption in blood, $\mu_{a,b}$, is more complicated,

$$\frac{\partial A}{\partial \mu_{a,b}} = p_d + \mu_{a,b} p'_d + \mu_{a,d} p'_d, \quad (7)$$

where $p'_d = \partial p_d / \partial \mu_{a,b}$. The first term corresponds to the basic Beer–Lambert law. The second term adds a nonlinear component due to the nonconstant pathlength. The third term is cross-talk from absorption of dermis to absorption of blood.

2.1 Diffusion Model

Equation (7) cannot be used for calculating concentration changes because p_d is not known. The model based on diffusion theory, introduced by Farrell et al.²⁴ and Patterson et al.,²³ can be used for obtaining the partial derivatives needed. The diffusion model assumes a pencil-beam-shaped light source. It is further assumed that the light beam can be replaced with a point source located at the depth of the mean free path, $z_0 = 1/(\mu'_s + \mu_a)$, under the skin surface and the corresponding image source at the height of $2z_b + z_0$ from the skin surface, where $z_b = (2K)D$ is the height of the virtual boundary, where K is the internal reflection, which is assumed to be $K = (1 + r_d)/(1 - r_d)$, where r_d is the reflectance coefficient mismatch in the air-tissue boundary and $D = z_0/3$ is the diffusivity coefficient. The diffusion reflectance can be modeled by means of transport albedo $\mu'_a = \mu'_s/(\mu'_s + \mu_a)$, and internal reflection K . A more accurate model is obtained by assuming that there is a point source in every point along the pencil beam in the tissue, in which intensity along the depth, z , is $I(z) = \mu'_a \mu'_t e^{-\mu'_t z}$, where $\mu'_t = \mu_a + \mu'_s$ is the total interaction coefficient. Therefore, the total reflectance, R_d , of infinite narrow beam is²⁴

$$R_d = \frac{\mu'_a}{2} \frac{1 + e^{-4/(3KT)}}{1 + T}, \quad (8)$$

where

$$T = \sqrt{3(1 - \mu'_a)}. \quad (9)$$

The absorption, A_d , of radiation in tissue is

$$A_d = \log(1/R_d). \quad (10)$$

The derivative of Eq. (10) by absorption coefficient, μ_a , is

$$\frac{\partial A_d}{\partial \mu_a} = \frac{z_0}{2(T+1)} \left[2(T+1) + \frac{3z_0 \mu'_s}{T} + \frac{4Kz_0 \mu'_s (T+1) e^{-4/(3KT)}}{T(e^{-4/(3KT)} + 1)} \right]. \quad (11)$$

The epidermis and dermis are the two most important layers for optical skin models. The dermis can be further subdivided, but it may not be always necessary. Here, the skin model assumes a thin epidermis layer situated on top of the dermis layer. The absorption in epidermis, A_e , is modeled simply using BLL, so that $A_e = \mu_{a,e} p_e$, where the average pathlength in epidermis, p_e , is slightly longer than the thickness of the epidermis, d_e . The absorption of dermis is modeled using the diffusion model, described in Eq. (10). The specular reflectance is assumed to be wavelength-independent constant.

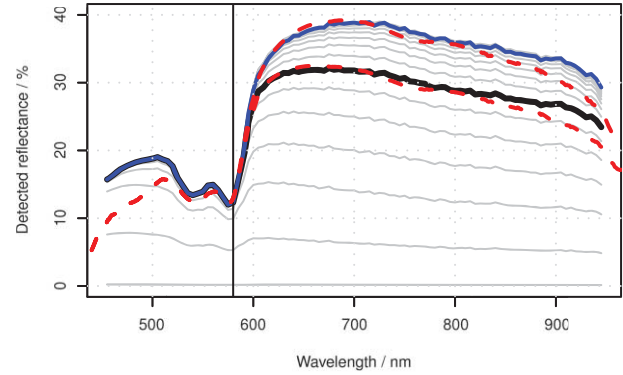


Fig. 1 Edge losses and edge-loss compensation. The gray lines show the detected reflectance as a function of wavelength, from bottom to top, r_a is 0, 0.1, 0.2, 0.3, ..., 1.5 cm. The lower solid thick line shows the simulated detected reflectance, whereas the lower thick dashed line shows measured spectra. The upper thick and dashed lines show the simulated and measured spectra after edge loss compensation.

2.2 Edge Losses

One of the data sets used in this paper is measured using an integrating sphere, which is often used as an optical probe for reflection measurements. However, it introduces some nonideal characteristics that must be taken into account. The integrating sphere illuminates the target at the area of its aperture, which is the radius r_a . It collects the specular and diffuse reflectance only from the area covered by the aperture. However, part of the diffuse reflectance is remitted from the area behind the edge of the aperture and part of the reflectance is therefore lost. To reduce edge losses, some integrating spheres contain a lens system that can be used either in focusing the illumination into a narrow collimated beam or limiting the detection area. To estimate the edge losses of an integrating sphere with a lens system used for illumination, an MCML simulation was performed with a collimated circular light beam of radius $r_b = 0.15$ cm and aperture of radius $r_a = 0.5$ cm, which are the properties of the integrating sphere used in the Allen's test measurements. The result of the MCML simulation is a radial cross section of the reflectance intensity. The intensity of the total collected reflectance can be obtained by integrating the reflectance intensity curve over a circle of radius r_a . The detected reflectance and the edge losses should be the same in a symmetrical case, where the integrating sphere is used for providing diffuse light in the circular area, of radius, r_a , and the lens system is used for limiting the detection in the circular area of radius, r_b . The results of the simulation are shown in Fig. 1.

The detection efficacy of the integrating sphere was calculated by dividing the reflectance obtained using the real aperture radius with the reflectance using very large aperture radius, capturing virtually all reflected signal,

$$\eta(\lambda) = \frac{R(\lambda)|_{r_a=0.6 \text{ cm}}}{R(\lambda)|_{r_a=1.5 \text{ cm}}}. \quad (12)$$

According to MCML simulation, the losses are negligible when wavelength, λ , is smaller than $\lambda_t = 580$ nm. When $\lambda > \lambda_t$, $\eta(\lambda)$ can be modeled as an exponent function. Therefore,

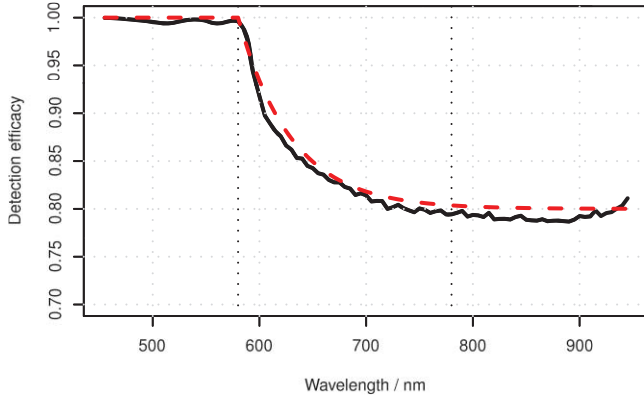


Fig. 2 Detection efficacy due to edge losses. The solid line shows the simulated detection efficacy and dashed line shows the detection efficacy model.

the detection efficacy is

$$\eta(\lambda) = \begin{cases} 1 & \text{if } \lambda \leq \lambda_t \\ E_L + (1 - E_L)e^{k(\lambda_t - \lambda)} & \text{if } \lambda > \lambda_t, \end{cases} \quad (13)$$

where E_L is the edge loss coefficient, describing the maximum detection efficacy in the NIR range, and k is an experimental constant. For simulated skin parameters and given integrating sphere geometry, $E_L = 0.8$ and $k = 0.02$. The simulated and modeled $\eta(\lambda)$ are shown in Fig. 2.

The detection efficacy model was further tested by plotting one spectra from the Allen's test data, before and after the edge loss compensation. These measured spectra are also shown in Fig. 1.

2.3 Total Skin Reflectance Model

The total absorption of the skin, when the diffusion model of the dermis, the Beer–Lambert model of the epidermis, the edge losses, and the specular reflections are taken into account, is shown in Fig. 3. The reflectance from epidermis to the air is assumed to be independent on the wavelength and is accounted for by increasing the specular reflection coefficient R_s . The scattering from epidermis to dermis is neglected in the model.

The parameters of the model are the specular reflection R_s , the absorption of the epidermis A_e , the absorption of the dermis A_d , and the edge loss coefficient E . From Eqs. (8) and (9), it is apparent that the absorption in Eq. (10) is directly determined by the internal reflectance of because K , and the transport albedo μ'_a . The transport albedo, in turn, is a sum of all absorption and scattering properties of skin because $\mu_a = \mu'_s / (\mu'_s + \mu_a)$. The absorption coefficient is a function of absolute chromophore concentrations, because $\mu'_a = \sum_i \varepsilon_i(\lambda)c_i$, where ε_i is the *a priori* known molar extinction coefficient of chromophore i . Therefore, the transport albedo can be calculated as follows:

$$\mu'_a(\lambda, \mathbf{c}) = \frac{\mu'_s(\lambda)}{\mu'_s(\lambda) + \sum_i \varepsilon_i(\lambda)c_i}, \quad (14)$$

where $\mathbf{c} = [c_1, c_2, \dots]^T$ is a vector containing the concentrations of all chromophores included in the model.

Because μ'_a is a function of λ and \mathbf{c} , so are $T(\lambda, \mathbf{c})$, $R_d(\lambda, \mathbf{c})$ and $A_d(\lambda, \mathbf{c})$ as well. The BLL model of epidermis is $A_e(\lambda, c_m)$

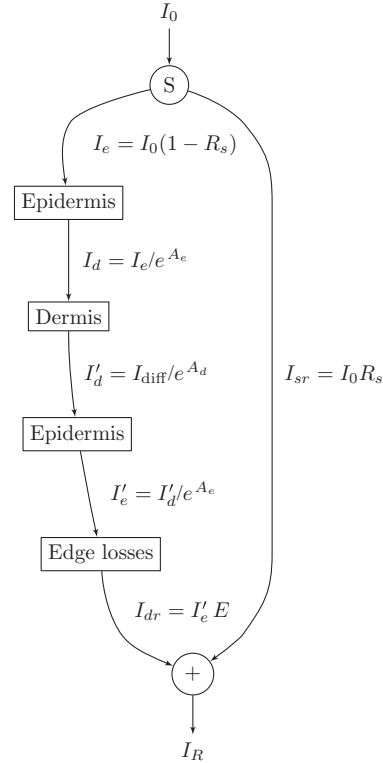


Fig. 3 Photon path model. The incident light beam, I_0 , is first divided in two parts, the diffuse reflected part, I_e , and the specularly reflected part, I_{sr} . The diffuse reflected beam, I_e , travels through epidermis and is partly absorbed. The transmitted part, I_d , enters into the dermis and is partly reflected back. The reflected intensity, I'_d , goes through epidermis the second time. The diffuse and specular reflections are collected by a detector, which potentially causes edge losses to the diffuse reflected part of light, I'_e . The absorption of epidermis, A_e , is calculated by the Beer–Lambert law and the absorption of dermis, A_d , is obtained from the diffusion theory.

$= \varepsilon_m(\lambda)c_m$. The parameters for the edge-loss model, $E(\lambda)$ are E_L and k . The total skin reflectance model can be used in solving the concentrations, by adapting it to the measured reflectance spectrum, by minimizing the following square error over all spectral channels, i :

$$E_{SS}(\mathbf{c}, R_s, E_L, k) = \sum_i [R_{\text{measured}}(\lambda_i) - R_{\text{predicted}}(\lambda_i, \mathbf{c}, R_s, E_L, k)]^2. \quad (15)$$

The E_{SS} can be minimized by finding optimal values for the parameters with LMA algorithm, for example. When the skin model is optimized, the derivative shown in Eq. (10) can be obtained.

The absorption difference between two locations of skin can now be written using Eqs. (6) and (11) as a Taylor series,

$$\Delta A = \frac{\partial}{\partial \mu_a} A (\Delta \mu_{a,b} + \Delta \mu_{a,d}) + 2p_c \Delta \mu_{a,c}. \quad (16)$$

The specular reflection is canceled when measuring the difference of two absorption spectra; therefore, it may be ignored. The possible edge loss needs to be compensated before applying Eq. (16). To keep the system linear, the higher order terms of the Taylor series cannot be used. The chromophore concentrations

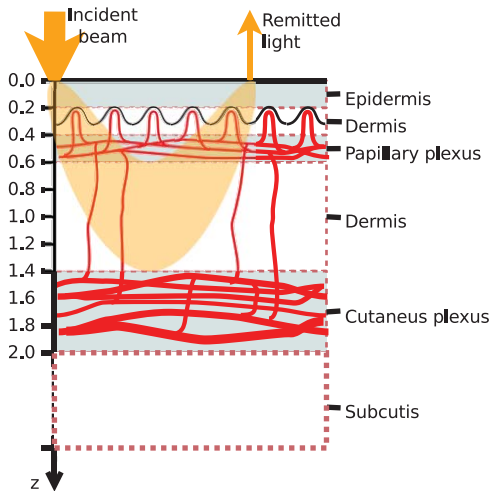


Fig. 4 MCML skin-simulation model structure. The depths of the layers in millimeters are given along z -axis, in the left hand side. The layers of the skin model are shown in the right hand side. The incident and remitted light beams are shown in the top. The banana-shaped area is a schematic of the typical path for the photons contributing to the remittance shown by the arrow.

can be solved when the absorption coefficients, μ'_a , are replaced by concentrations and extinction coefficients,

$$\Delta A = \frac{\partial}{\partial \mu_a} A (\Delta c_{\text{HbO}} \varepsilon_{\text{HbO}} + \Delta c_{\text{Hb}} \varepsilon_{\text{Hb}} + \Delta c_{\text{base}} \varepsilon_{\text{base}}) + 2p_e \Delta c_m \varepsilon_m. \quad (17)$$

Equation (17) contains four unknown concentrations. They can be solved by measuring the absorption change, ΔA , in at least at four different wavelengths, and finding an least-mean-squares (LMS) solution for each absorption. The wavelengths should be selected so that the equations are linearly independent. This can be arranged by selecting the wavelength sufficiently far away from each other. The absorption coefficients have unique spectra because they depend on the spectra of the extinction coefficients, ε .

2.4 Reference Data Using Monte Carlo Simulation

To validate the proposed chromophore mapping technique, it was compared to the MCML simulation model. The MCML model consists of the model structure and the parameters. The structure is assumed to consist of homogeneous layers (shown in Fig. 4). The model was originally developed by Tuchin et al.,³³ adopted by Reuss,¹⁵ and used, among others, by us.^{20,22,34}

The parameters of each layer are the thickness, d , the absorption coefficient, μ_a , the scattering coefficient, μ_s , and the anisotropy, g . To be able to estimate the absorption coefficients, the skin chromophores and their concentrations are needed. In addition to hemoglobin and melanin, bilirubin and β -carotene may also affect to the concentration prediction. Water is only significant above 800 nm; it does not influence the skin color. The skin model was tuned to match palm skin over a range of different blood concentrations using the Allen's test, as described in Ref. 34. The nominal blood concentration is 150 g/l. The

hemoglobin molar concentration in blood can therefore be calculated by dividing the concentration in grams/liter with the molar mass of hemoglobin; therefore,

$$c_{\text{Hb,blood}} = \frac{150 \text{ g/l}}{64500 \text{ g/mol}} = 2.326 \text{ mol/l}. \quad (18)$$

The concentration of hemoglobin in skin is obtained by multiplying the hemoglobin concentration with the amount of blood in skin, the blood fraction, f_b . Therefore,

$$C_{\text{Hb,skin}} = f_b C_{\text{Hb,blood}}. \quad (19)$$

The typical value for f_b was 0.05 according to Reuss in Ref. 15. We have observed lower f_b values in our earlier studies, including, Ref. 34 where $f_b \in [0.0016, 0.0045]$.

Often the absorption coefficient of melanin is modeled as follows:

$$\mu_{a,m} = f_m (1.70 \times 10^{12}) \lambda^{-3.48} \quad (1/\text{cm}), \quad (20)$$

where λ is the wavelength in nanometers. The melanin fraction, f_m , is estimated instead of estimating the concentration of melanin molecules.³⁵ This is because the size, structure, and the absorption efficiency of the melanin molecules may vary. Therefore, the absorption coefficient for given melanin concentration is not well defined.

The scattering of the tissue was modeled as a combination of Mie and Rayleigh scattering, as follows:³⁶

$$\begin{aligned} \mu_s(\lambda) &= \mu_{s,\text{Mie}}(\lambda) + \mu_{s,\text{Rayleigh}}(\lambda) \\ &= 2 \times 10^5 \times \lambda^{-15} + 2 \times 10^{12} \times \lambda^{-4.0}. \end{aligned} \quad (21)$$

The skin without blood, the skin baseline, was simulated using following formula:³⁷

$$\mu_{a,d}(\lambda) = 7.84 \times 10^8 \times \lambda^{-3.255} \quad (22)$$

The variations in bilirubin concentration can potentially disturb the prediction of hemoglobin concentration or oxygen saturation. Therefore, the bilirubin concentration was varied in MCML simulation even though the prediction of the bilirubin content was not tried. The nominal bilirubin concentration in blood is $C_{\text{Br}} = 10 \mu\text{M/l}$. The bilirubin concentration was kept constant during "Blood" and "Melanin" data set simulation, and random values between the range, shown in Table 1 were selected in the simulation of the "Random" data set.

The above skin model is used to generate four data sets, described in Table 1. The first two data sets are used for obtaining the numerical derivative of absorption by the melanin or blood concentrations for reference. The melanin set, contains 32 simulated skin spectra where all variables, except melanin concentration were kept constant. The melanin concentration was linearly distributed within a given range. In the blood data set, which also contains 32 simulated spectra, all variables except blood volume fraction, f_b , were kept constant. The blood fraction, f_b , was a linearly distributed within a given range. The random data set contains 104 simulated spectra, where independent random values were selected for melanin and blood concentrations from the given ranges.

Table 1 Simulated data sets and the range of the parameters during the simulation.

Data-set name	Number of samples	Range
Melanin	32	$f_m \in [0.01, 0.04]$ $f_b = 0.005$ $O_s = 0.8$ $C_{Br} = 10 \mu\text{M}/1$
Blood	32	$f_m = 0.02$ $f_b \in [0.0, 0.010]$ $O_s = 0.8$ $C_{Br} = 10 \mu\text{M}/1$
Random	104	$f_m \in [0.0, 0.05]$ $f_b \in [0.0, 0.025]$ $O_s \in [0.6, 1]$ $C_{Br} \in [2.5, 25] \mu\text{M}/1$

Each simulated spectra, in each data set, contains 78 wavelengths in the range $\lambda \in [380, 1050]$ nm. The simulations were made by tracking 10^6 photons for each simulated wavelength. The plain MCML simulation estimates the reflectance of an infinite thin pencil beam.

2.5 Allen's Test Data

In addition to the simulated data, the proposed algorithm was also validated using a measured data set. The measured data set consists of the reflectance spectra of the human skin from the palm of the hand from 20 persons, 5 locations each. From each location, a series of 10 consequent samples were measured at the rate of ~ 1.8 samples per second. The measurements were carried out using an HR4000 spectrometer (Ocean Optics, Dunedin, Florida) and an ISP-REF integrating sphere (Ocean Optics). The measurement of the reflectance of the palm was acquired so that the test person placed his or her hand very lightly on the integrating sphere. The skin was illuminated with a diffuse light field over the whole aperture of the sphere, in which radius $r_a = 0.5$ cm, using a light source, built in the sphere. The reflectance was collected in the middle of the aperture, from the circular area, in which the radius is $r_b = 0.15$ cm. The experiment is further described in Ref. 34.

3 Results

3.1 Numerical Versus Analytical Derivatives

To validate the analytical derivatives shown in Eqs. (6) and (11), they were compared to corresponding numerical derivatives obtained from the MCML data sets, melanin and blood, shown in Table 1. These data sets contain the absorption spectra when

a single-chromophore concentration, either melanin or blood, is perturbed within a range, and all other parameters are kept unchanged. A third-order polynomial was fitted to the simulated $A(c)$ curves, using statistical software package, R, and functional data analysis toolbox.³⁸ The derivatives of $A(c)$ were now easily obtained by differentiating the corresponding polynomials. To study these polynomials and the first-order derivative over full reflectance spectra, the absorptions were differentiated by the concentrations instead of the absorption coefficients, and the procedure was repeated over the spectral range of $\lambda \in [380, 1050]$ nm. The derivative of the absorption, A , by the absorption coefficient μ , and the derivative by the concentration are directly related because

$$\frac{\partial}{\partial \mu} A(\lambda, \mu) = \frac{1}{\varepsilon(\lambda)} \frac{\partial}{\partial c} A(\lambda, c). \quad (23)$$

The simulation results for Eq. (5) as a function of varying melanin concentrations are shown in Fig. 5(a). The polynomial was fitted to the measured values of absorption as a function of melanin concentration, $A(c_m)$, at each wavelength. Figure 5(b) displays the coefficients of the $A(c_m)$ polynomial over all wavelengths.

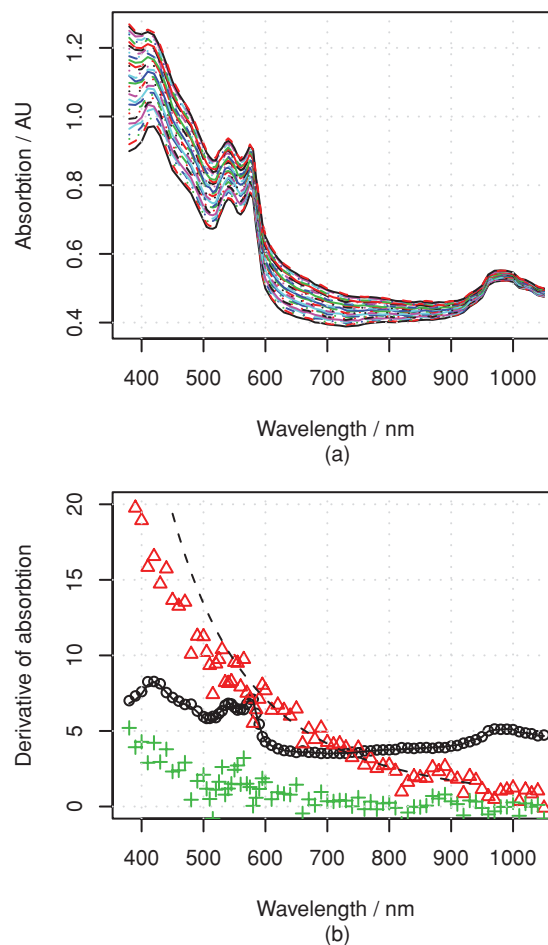


Fig. 5 Absorption of skin by varying melanin fraction, f_m . (a) Absorption when the melanin fraction is increased from 1 to 4% in even steps of 0.095%. (b) Zeroth- (O), first- (Δ), and second- (+) order coefficients (not in scale) of the fitted polynomial $A(c_m)$. The solid line shows the absorption when $c_m = 0$, and the dashed line shows the analytical derivative $\partial A / \partial \mu_{a,m}$.

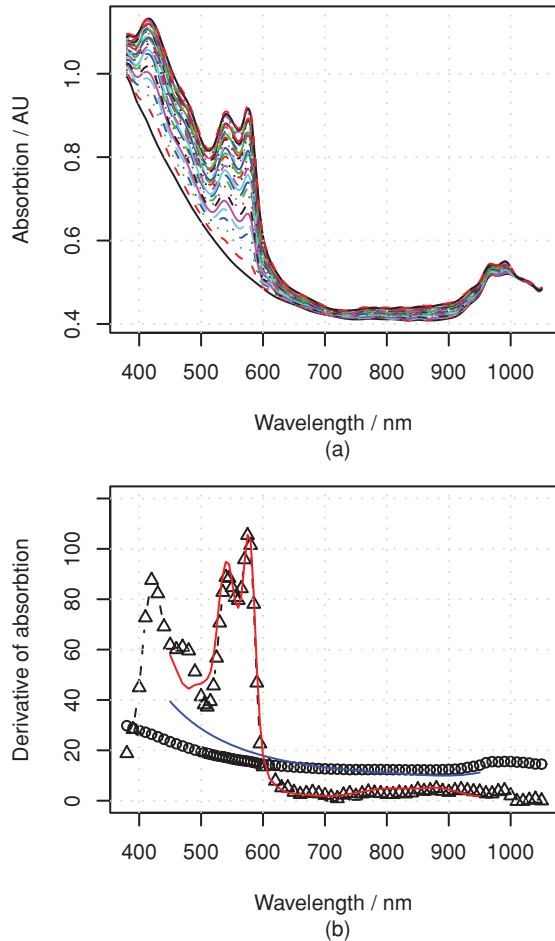


Fig. 6 Absorption of skin with varying blood concentration. (a) Absorption when the skin blood fraction is increased from 0 to 1% in even steps of 0.031%. (b) Zeroth- (O) and first- (Δ) order coefficients of the fitted polynomial $A(c_m)$ (zeroth-order polynomials is multiplied by 30), the coefficients of the absorption polynomial, A , by blood concentration c_b . The solid line shows the corresponding analytical derivative.

The zeroth-order coefficient of the polynomial and the skin absorption without melanin are, as expected, very close to each other. Correspondingly, the first-order coefficient and the analytical derivative are similar when the wavelength, $\lambda > 550$ nm. The numerical estimate is noisy, making the root-mean-square error-percentage (RMSEP) difference as large as 14%. For wavelengths at <550 nm, the behavior deviates from the Beer–Lambert law. The assumption of constant pathlength does not hold any longer because the absorption of melanin becomes very strong. The values of the second-order coefficient also seem to deviate from zero at wavelengths shorter than 550 or even 600 nm. The simple model shown in Eq. (6) seems work better at longer wavelengths.

3.2 Absorption Versus Blood Concentration

The simulation results for Eq. (5) and the comparison to Eq. (11) are shown in Fig. 6. The constant term and the skin absorption without blood are significantly different at short wavelengths. This is because in addition to the linear term p_d , the derivative also contains the nonlinear blood effect, $\mu_{a,b}p'_d$, and the cross-talk between skin baseline, $\mu_{a,d}p'_d$. The numerical and an-

alytical first-order derivatives are again similar (<550 nm). The explanation for larger differences in the range 450–500 nm is the absorption of bilirubin. Bilirubin was assumed to be solved in blood in MCML simulation but not in the diffusion model. Therefore, the derivative of MCML data contains also the absorption of bilirubin, but the diffusion model does not. This difference did not seem to significantly disturb the prediction of blood and melanin concentrations.

3.3 Comparison to Monte Carlo Simulation

The accuracy of the prediction of the chromophore concentrations is assessed by means of the random MCML simulation data set, shown in Table 1. The results are displayed in Fig. 7. The accuracy of the prediction is measured as the RMSEP

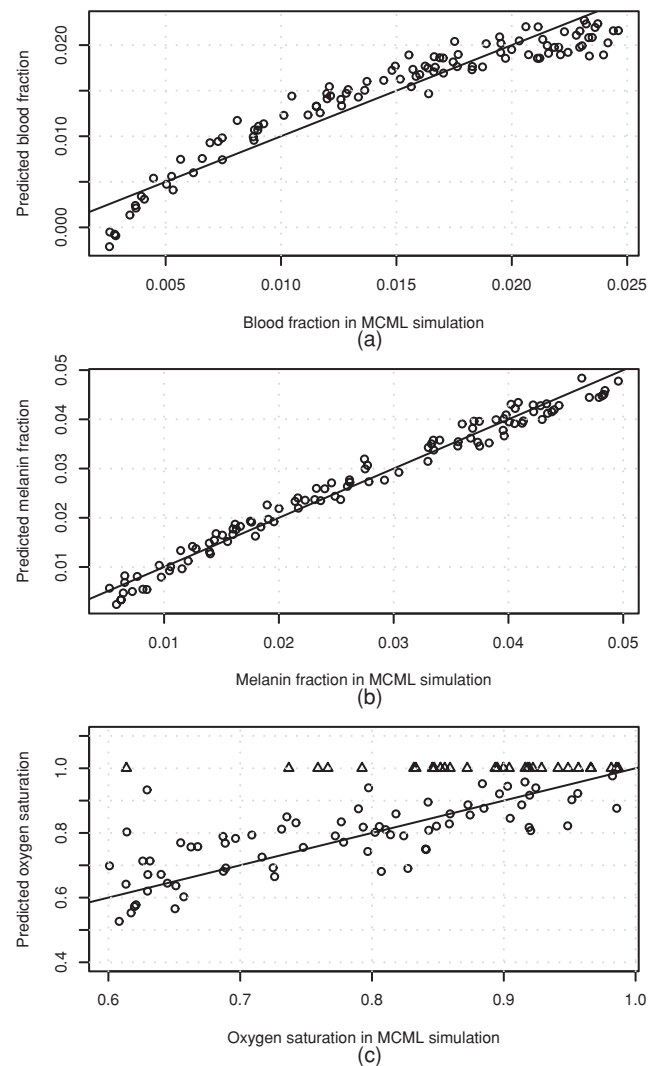


Fig. 7 Prediction of the chromophore concentrations of the MCML simulation using dMBLL and following wavelengths: $\lambda \in \{505, 530, 595, 625, 850\}$ nm. (a) Predicted blood fraction against blood fraction used in the MCML simulation. The prediction error is RMSEP=15% and the correlation between predicted and given values, $r=0.94$. (b) Predicted fraction of melanin against the melanin fraction used in MCML simulation. The prediction error RMSEP=7% and correlation $r=0.99$. (c) Predicted oxygen-saturation levels against saturation levels in the MCML simulation. RMSEP=10%, $r=0.73$.

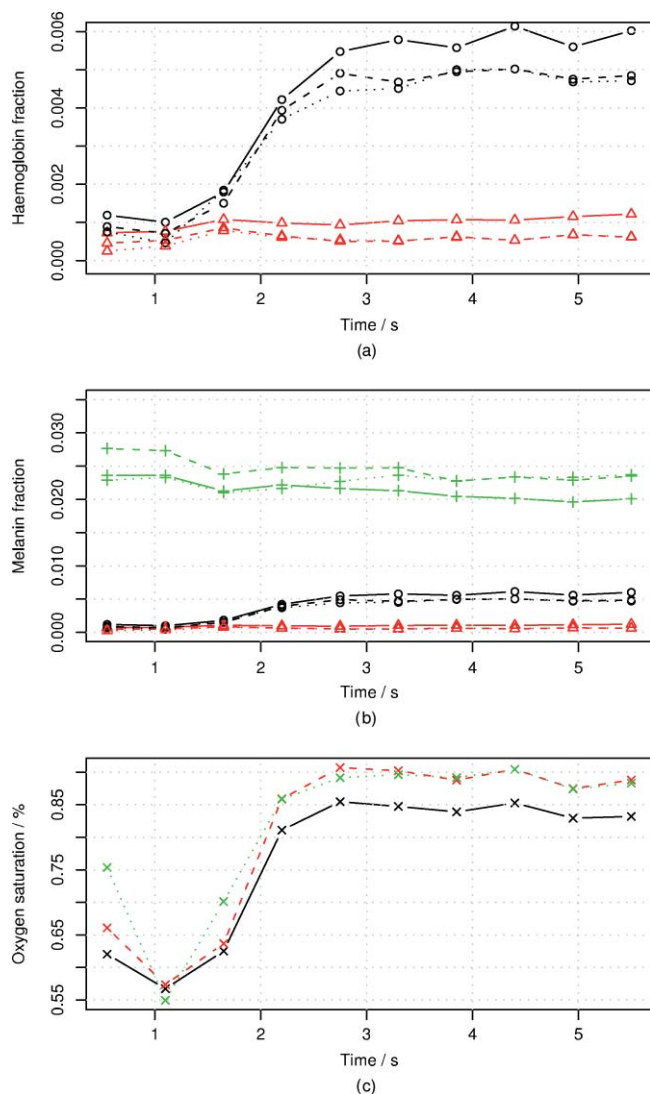


Fig. 8 Predictions of the chromophore concentrations of the Allen's test data set. Solid lines are predictions made by fitting the diffusion model to the full spectra. Dashed lines are obtained by fitting the diffusion model to selected five wavelengths, $\lambda \in \{505, 530, 595, 625, 850\}$ nm. The predictions shown in the dotted lines are obtained by fitting the dMBLL model to the difference of the spectra. The reference spectrum is the one measured at time $T = 4.4$ s. (a) Fraction of oxyhemoglobin (o) in upper curve and the fraction of deoxyhemoglobin (Δ) in lower curve, (b) Predicted fraction of melanin (+) in skin, and (c) Predicted oxygen saturation levels.

error and Pearson correlation coefficient between the predicted and given values. The prediction of the melanin content is the most accurate. Blood-prediction performance is slightly weaker than prediction for melanin because the relationship between the blood concentration and absorption is curved. The prediction of oxygen saturation is the weakest. Often the concentration of deoxyhemoglobin is very low, and even small absolute errors cause large relative errors. Sometimes even slightly negative values were observed. If negative concentration was observed, then it was saturated to zero. The samples shown as triangles are these kinds of fixed predictions.

Table 2 The Speeds of different implementations.

Method	Number of wavelengths	Execution time/spectrum	Time for 1 megapixel
MCML	285	25 min	NA
MCML	5	26 s	NA
Diffusion	285	1.1 s	12 days
Diffusion	5	0.53 s	6 days
dMBLL	5	1.2 ms	20 min

3.4 Allen's Test Data

The algorithm was applied to the experimental Allen's test data to study its performance for measured data. The results are shown in Fig. 8. The prediction of each chromophore was done with three different methods. First by fitting the skin model to the spectra by optimizing the chromophore concentrations with LMA (solid line). Then the same method was repeated, but now only five selected wavelengths were used (dashed lines). The third method is to use the analytical derivative and Eq. (17) to solve the linearized skin model around an operating point. The spectrum measured at time $T = 4.4$ s was used as an operating point.

3.5 Execution Speed

To evaluate the speed benefit gained by using a closed-form dMBLL solution, the predictions done above were benchmarked. The diffusion model and the dMBLL implementations were programmed with a statistical software package, called R. The MCML program was programmed with C. The predictions were run in a normal desktop PC. The processor of the PC was Intel®Core 2 CPU 6600 using a 2.40-GHz clock frequency. We also estimated how long it would take to process every pixel in a 1-megapixel image. The results of the benchmarks are shown in Table 2.

4 Discussion

The absolute blood concentration in dermis is perhaps not a clinically significant parameter because it varies all the time. The local and global blood circulation regulation change the blood perfusion in skin due to body and ambient temperature changes, due to physical exercise and the activity of metabolism, and for many other reasons not directly related to skin. Therefore, we have used the difference of the absorption between the normal skin and a skin disorder in measuring the severity of the disorder. The method developed here, represented by Eq. (17) can be used for finding the corresponding difference in chromophore concentrations behind the change of absorption. However, the absolute concentrations in the reference area are also needed because the derivative of absorption of dermis [shown in Eq. (10)] depends on the absolute concentration.

The fitting of the diffusion model to the average spectra of normal skin using LMA is a suitable method for determining

the normal operating point, around which the skin absorption can be linearized. The proposed method forms a simple relationship between the chromophore concentrations and the absorption. Many similar methods are based on heuristics of the shape of the spectral curves. Our method is based on solving a simple matrix equation where the transformation matrix is calculated from the analytical derivatives of the diffusion model. The method can be easily adapted to any set of chromophores and arbitrary wavelengths. The transformation matrix is optimized case by case. The numerical derivative of the MCML model could be used as well, but it is much slower to compute. The proposed model is accurate near the operating point, but the error increases when the difference in chromophore concentration becomes larger. The accuracy of the measurement may be further increased by using several reference points, in case the difference of concentrations is abnormally high.

The method can adapt to different wavelengths, but the accuracy is different in different wavelengths. The five wavelengths used in this paper form one good subset of wavelengths, because the accuracy is sufficient and they can all be produced using commonly available light-emitting diodes. Therefore, a spectral imaging system for chromophore mapping can be easily constructed. The accuracy may be still improved by optimizing the wavelengths. The proposed model should not be used for wavelengths of <550 nm because the model of epidermis differs significantly from MCML simulation. More research is needed to correct this problem in the future.

Here, the model also takes into account the specular reflections from the surface of the skin. In practice, the specular reflection can vary between skin locations, causing additional error. These reflections can be removed from the image by placing a polarizing filter in front of the light source and placing the second filter orthogonally in front of the camera lens, as described in Ref. 25 (Chap. 7). In this way, specular reflections and single scattered photons are filtered away. The polarization of the multiple scattered photons is lost, and therefore, part of them will pass through a second filter into the camera. When using these cross-polarizing filters, special attention must be paid to calibration, because the typical white references may reflect light mainly retaining the polarization. Therefore, the camera may measure even higher reflectance for red and NIR from skin than from the white reference.

The execution speeds of the optimization methods are unsuitably slow to the chromophore mapping purposes at the resolutions of contemporary cameras. The LMS algorithm is fast enough, but then the system needs to be linearized. When the system is linearized around a proper operating point, case by case, the linearization does not cause too much error.

The proposed method for compensating the edge losses of the integrating sphere works for the optical properties used in the MCML simulation. However, the method is not validated for optical scattering and absorption coefficients, which differ significantly from those of normal skin. The simulations cover only one probe geometry, where light is illuminated through a collimated beam, which radius $r_b = 0.15$ cm, and the aperture radius of the integrating sphere was $r_a = 0.5$ cm. More studies are needed to find out if it is enough to only optimize the model parameters E_L and k or change the whole model, when the probe geometry changes.

5 Conclusion

In this research, a method is proposed to build a linear model, based on the differential Beer–Lambert law to efficiently map the chromophore concentrations in the spectral image of human skin. The proposed algorithm calculates an optimal linear model around an operating point, taking into account the spectra of the selected wavelengths, the concentrations of these chromophores in the selected operating point, and the available wavelengths. The system is validated against a data set created with a MCML simulation and a spectrometer measurement during the Allen’s test, which modulates the blood fraction in skin.

The accuracy of the measurement is good enough for many purposes. The RMSEP in predicting the blood and melanin fraction was correspondingly 15 and 7%, and the Pearson correlation coefficients were $r = 0.94$ and $r = 0.99$. The prediction of the oxygen saturation is more error prone because the concentration of the deoxygenated hemoglobin is small. Therefore, the prediction of the oxygen-saturation levels is more difficult and the Pearson correlation between given and predicted values is $r = 0.73$. The error percentage is still low: RMSEP = 10% because the oxygen saturation levels were only predicted in the range of $O_s \in [0.6, 1.0]$, and therefore, the errors are small compared to the actual value.

The proposed method is orders of magnitude faster than the methods based on optimization during prediction. Therefore the rendering of high-resolution spectral images is also possible.

Acknowledgments

The authors wish to thank an anonymous proofreaders of Journal of Biomedical Optics. The received comments were very constructed and helped to further improve the article.

References

1. I. Konishi, Y. Ito, N. Sakauchi, M. Kobayashi, and Y. Tsunazawa, “A new optical imager for hemoglobin distribution in human skin,” *Opt. Rev.* **10**, 592–595 (2003).
2. D. Jakovels and J. Spigulis, “2-D mapping of skin chromophores in the spectral range 500–700 nm,” *J. Biophoton.* **3**, 125–129 (2010).
3. T. Yamamoto, H. Takiwaki, S. Arase, and H. Ohshima, “Derivation and clinical application of special imaging by means of digital cameras and ImageJ freeware for quantification of erythema and pigmentation,” *Skin Res. Technol.* **14**, 26–34 (2008).
4. I. S. Kaartinen, P. O. Valisuo, J. T. Alander, and H. O. Kuokka-nen, “Objective scar assessment—a new method using standardized digital imaging and spectral modelling,” *Burns* **37**(1), 74–81 February 2011.
5. M. Kobayashi, Y. Ito, N. Sakauchi, I. Oda, I. Konishi, and Y. Tsunazawa, “Analysis of nonlinear relation for skin hemoglobin imaging,” *Opt. Express* **9**, 802–812 (2001).
6. P. Clarys, K. Alewaeters, R. Lambrecht, and A. O. Barel, “Skin color measurements: comparison between three instruments: the Chromameter[®], the DermaSpectrometer[®] and the Mexameter[®],” *Skin Res. Technol.* **6**, 230–238 (2000).
7. L. E. Dolotov, Y. P. Sinichkin, V. V. Tuchin, S. R. Utz, G. B. Altshuler, and I. V. Yaroslavsky, “Design and evaluation of a novel portable erythema-melanin-meter,” *Lasers Surg. Med.* **34**, 127–135 (2004).
8. M. Moncrieff, S. Cotton, E. Claridge, and P. Hall, “Spectrophotometric intracutaneous analysis: a new technique for imaging pigmented skin lesions,” *Br. J. Dermatol.* **146**, 448–457 (2002).
9. G. E. Nilsson, H. Zhai, H. P. Chan, S. Farahmand, and H. I. Maibach, “Cutaneous bioengineering instrumentation standardization: the tissue viability imager,” *Skin Res. Technol.* **15**, 6–13 (2009).

10. G. V. G. Baranoski and A. Krishnaswamy, "Light interaction with human skin: from believable images to predictable models," in *Siggraph Asia 08*, ACM, New York, pp. 1–80 (2008).
11. T. Igarashi, K. Nishino, and S. Nayar, "The appearance of human skin: A survey," *Found. Trends Comput. Graphics Vis.* **3**, 1–95 (2007).
12. S. A. Prahl, M. Keijzer, S. L. Jacques, and A. J. Welch, "A Monte Carlo model of light propagation in tissue," *Dosim. Laser Radiat. Med. Biol.* **IS 5**, 102–111 (1989).
13. L. Wang, S. L. Jacques, and L. Zheng, "MCML—Monte Carlo modeling of light transport in multi-layered tissues," *Comput. Methods Prog. Biomed.* **47**, 131–146 (1995).
14. L. H. Wang, S. L. Jacques, and L. Q. Zheng, "CONV—Convolution for responses to a finite diameter photon beam incident on multi-layered tissues," *Comput. Methods Prog. Biomed.* **54**, 141–150 (1997).
15. J. L. Reuss, "Multilayer modeling of reflectance pulse oximetry," *IEEE Trans. Biomed. Eng.* **52**, 153–159 (February 2005).
16. E. Claridge, S. Cotton, P. Hall, and M. Moncrieff, "From colour to tissue histology: physics based interpretation of images of pigmented skin lesions," in *Medical Image Computing and Computer-Assisted Intervention—MICCAI 2002*, Lecture Notes in Computer Science, Vol. 2488, Takeyoshi Dohi and Ron Kikinis, Eds., pp. 730–738, Springer Berlin (2002).
17. E. Claridge and S. Preece, "An inverse method for the recovery of tissue parameters from colour images," in *Processing in Medical Imaging*, Vol. 2732, pp. 306–317, Springer, Ambleside, UK (2003).
18. S. J. Preece and E. Claridge, "Spectral filter optimization for the recovery of parameters which describe human skin," *IEEE Trans. Pattern Anal. Mach. Intell.* **26**, 913–922 (July 2004).
19. M. Shimada, Y. Yamada, M. Itoh, and T. Yatagai, "Melanin and blood concentration in human skin studied by multiple regression analysis: experiments," *Phy. Med. Biol.* **46**, 2385–2395 (2001).
20. P. Valisuo, T. Mantere, and J. Alander, "Solving optical skin simulation model parameters using genetic algorithm," in *Proc. of 2nd Int. Conf. on BioMedical Engineering and Informatics*, pp. 376–380 (2009).
21. M. J. C. van Gemert, S. L. Jacques, H. J. C. M. Sterenborg, and W. M. Star, "Skin optics," *IEEE Trans. Biomed. Eng.* **36**, 1146–1154 (December 1989).
22. P. Välisuo and J. Alander, "The effect of the shape and location of the light source in diffuse reflectance measurements," in *Proc. of 21st IEEE Int. Symp. on Computer-Based Medical Systems*, IEEE Computer Society, pp. 81–86 (2008).
23. M. S. Patterson, B. Chance, and B. C. Wilson, "Time resolved reflectance and transmittance for the noninvasive measurement of tissue optical properties," *Appl. Opt.* **28**, 2331–2336 (1989).
24. T. J. Farrell, M. S. Patterson, and B. Wilson, "A diffusion theory model of spatially resolved, steady-state diffuse reflectance for the noninvasive determination of tissue optical properties *in vivo*," *Med. Phys.* **19**, 879–888 (1992).
25. V. V. Tuchin, *Tissue Optics: Light Scattering Methods and Instruments for Medical Diagnosis*, SPIE Press, Bellingham, WA (2007).
26. M. Shimada, Y. Masuda, Y. Yamada, M. Itoh, M. Takahashi, and T. Yatagai, "Explanation of human skin color by multiple linear regression analysis based on the modified Lambert–Beer law," *Opt. Rev.* **7**, 348–352 (2000).
27. L. Kocsis, P. Herman, and A. Eke, "The modified Beer–Lambert law revisited," *Phy. Med. Biol.* **51**, N91–N98 (2006).
28. M. G. Sowa, A. Matas, B. J. Schattka, and H. H. Mantsch, "Spectroscopic assessment of cutaneous hemodynamics in the presence of high epidermal melanin concentration," *Clin. Chim. Acta* **317**, 203–212 (2002).
29. G. N. Stamatas, B. Z. Zmudzka, N. Kollias, and J. Z. Beer, "In vivo measurement of skin erythema and pigmentation: new means of implementation of diffuse reflectance spectroscopy with a commercial instrument," *Br. J. Dermatol.* **159**, 683–690 (2008).
30. J. R. Mourant, T. M. Johnson, G. Los, and I. J. Bigio, "Non-invasive measurement of chemotherapy drug concentrations in tissue: preliminary demonstrations of *in vivo* measurements," *Phys. Med. Biol.* **44**, 1397–1418 (1999).
31. A. Amelink and H. J. C. M. Sterenborg, "Measurement of the local optical properties of turbid media by differential path-length spectroscopy," *Appl. Opt.* **43**, 3048–3054 (2004).
32. I. S. Kaartinen, P. O. Valisuo, V. Bochko, J. T. Alander, and H. O. Kuokkanen, "How to assess scar hypertrophy? A comparison of subjective scales and spectrocutometry — a new objective method," *Wound Repair Regen.* (in press).
33. V. V. Tuchin, S. R. Utz, and I. V. Yaroslavsky, "Tissue optics, light distribution, and spectroscopy," *Opt. Eng.* **33**, 3178–3188 (October 1994).
34. P. Valisuo, I. Kaartinen, H. Kuokkanen, and J. Alander, "The colour of blood in skin: a comparison of Allen's test and photonics simulations," *Skin Res. Technol.* **16**, 390–396 (November 2010).
35. S. L. Jacques and D. J. McAuliffe, "The melanosome: threshold temperature for explosive vaporization and internal absorption coefficient during pulsed laser irradiation," *Photochem. Photobiol.* **53**, 769–775 (1991).
36. S. L. Jacques, "Origins of tissue optical properties in the UVA, visible, and NIR regions," *Adv. Opt. Imaging Photon Migrat.* **2**, 364–369 (1996).
37. I. S. Saidi, "Transcutaneous optical measurement of hyperbilirubinemia in neonates," PhD Thesis, Rice University, Houston (1992).
38. J. O. Ramsay and B. W. Silverman, "Functional data analysis," *Stat. Comput.* **8**, 401–403 (1998).